Spatially varying phytoplankton seasonality on the Northwest Atlantic Shelf: A model-based assessment of patterns, drivers and implications

Zhengchen Zang[1], Rubao Ji[1], Zhixuan Feng[2], Changsheng Chen[3], Siqi Li[3], Cabell S. Davis[1]

[1] Department of Biology, Woods Hole Oceanographic Institution, Woods Hole, MA, USA

[2] State Key Laboratory of Estuarine and Coastal Research, School of Marine Sciences, East China Normal University, Shanghai, China

[3] School for Marine Science and Technology, University of Massachusetts Dartmouth, New Bedford, MA, USA

Corresponding author: Zhengchen Zang (Email: zzang@whoi.edu; Tel: 225-421-4719)

Key Words:

Gulf of Maine; Mid-Atlantic Bight; marine ecosystem modeling; phytoplankton seasonality; spatial heterogeneity; thermal sensitivity

Abstract

Signals of phytoplankton responses to climate-related forcing can be obscured by the heterogeneity of shelf seascapes, making them difficult to detect from spatiotemporally fragmented observations. In this study, a physical-biological model was applied to the Northwest Atlantic Shelf (NAS) to capture the seasonality of phytoplankton in terms of biomass and size composition. The difference in phytoplankton seasonality between the Mid-Atlantic Bight (MAB) and the Gulf of Maine (GoM) is a result of the interplay between nutrients and temperature: In the MAB, relatively high temperature in the cold season and longer duration of oligotrophic environment in the warm season contribute to an earlier winter bloom and a later fall bloom; In the GoM, low temperature and strong mixing limit phytoplankton growth from late fall to early spring, resulting in a later spring bloom and an earlier fall bloom. Although the temperature difference between the GoM and the MAB is likely to decrease in the future, stratification and surface nutrient regimes in these two regions will remain different owing to distinct thermohaline structures and deep-water intrusion. The spatial heterogeneity of phytoplankton dynamics affects regional pelagic and benthic production through connections with zooplankton and benthic-pelagic coupling.

1. Introduction

The Northwest Atlantic Shelf (NAS) from the Gulf of Maine (GoM) to the Mid-Atlantic Bight (MAB) has long been recognized as a highly productive ecosystem, providing essential habitat for breeding, spawning, and feeding of abundant marine life (Mills et al., 2013; Goode et al., 2019). As the foundation of the pelagic food web, phytoplankton supports the marine ecosystem by converting inorganic carbon and nutrients to organic compounds. On the NAS, the seasonality of phytoplankton dynamics plays an important role in nutrient cycling and the

phenology of higher trophic levels (Staudinger et al., 2019). Therefore, a comprehensive understanding of phytoplankton dynamics at the seasonal time scale and its spatial heterogeneity is essential for detecting the impacts of climate-forced ecosystem changes and supporting ecosystem-based fisheries management.

Nitrogen is a predominant limiting nutrient for phytoplankton growth in the NAS ecosystem, and its seasonal variation in the euphotic layer is modulated by stratification and mixing (O'Reilly and Busch, 1984; Townsend et al., 2006). New nitrogen over the NAS is provided by terrestrial discharge, atmospheric deposition, and inflow from the open ocean (Townsend et al., 2010; Zhang et al., 2013; Friedrichs et al., 2019). In the GoM, the intrusion of slope water through the Northeast Channel acts as a major source of dissolved inorganic nitrogen (Ramp et al., 1985; Townsend et al., 2010). After entering the GoM, nutrient-rich deep waters are brought to the surface via multiple physical processes (e.g., tidal mixing, upwelling, and convective overturning). Fluvial discharge is another source of new nitrogen in the GoM nearshore areas with limited offshore expansion (Townsend et al., 2010). Compared with new nitrogen from external reservoirs, internally recycled nitrogen in the GoM has gained more attention recently, with both model results and field measurements suggesting its importance in supporting surface productivity (Townsend, 1998; Switzer et al., 2020). In the MAB, the impact of terrestrial nutrient fluxes is also largely limited to nearshore areas, although the contribution of nutrient load from large estuarine systems is higher than that in the GoM (Fennel et al., 2006; Zhang et al., 2019). Over the shelf break, cross-frontal mixing events between slope and shelf waters provide additional nitrogen flux into the MAB (Malone et al., 1983; Townsend et al., 2006; Friedrichs et al., 2019).

Phytoplankton dynamics over the NAS are characterized by pronounced seasonality and spatial heterogeneity. In the GoM, phytoplankton have a major bloom in winter-spring and a secondary bloom in fall (Thomas et al., 2003). Lower chlorophyll concentration in summer is due to surface nutrient depletion associated with strong vertical stratification (Tian et al., 2014; Li et al., 2015). Both observations and model results indicate that surface freshening due to Scotian Shelf Water (SSW) inflow has likely enhanced vertical stratification and contributed to an earlier spring bloom with reduced magnitude in the GoM (Ji et al., 2007, 2008b; Song et al., 2010). In fall, nutrient replenishment from weakened stratification fuels the secondary bloom, and the interannual variability of its formation is related to vertical mixing and pre-bloom conditions (Hu et al., 2011). In the MAB, the seasonal variation of phytoplankton is out of phase with that in the GoM: the winter bloom on the inner shelf of the MAB occurs prior to the spring bloom in the GoM (Yoder et al., 2001; Xu et al., 2011). The timing and magnitude of phytoplankton biomass accumulation in the MAB are largely controlled by water stratification (Xu et al., 2011).

The size structure of phytoplankton communities can affect the efficiency and fate of primary production, and its seasonality can be influenced by physical-biogeochemical conditions on the shelf, including vertical mixing, wind, light, temperature, and nutrient availability (Mouw and Yoder, 2005, 2010). Overall, the eutrophic environment favors high abundance of large phytoplankton (e.g., diatom). In the GoM, both field measurements and satellite data indicate that mixing-induced strong nutrient replenishment in winter results in the dominance of diatoms during winter-spring, and community cell size decreases from nearshore area to deep basins as the nutrient availability reduces seaward (Mouw and Yoder, 2005; Townsend et al., 2010; Pan et al., 2011). During the summer season, small phytoplankton (e.g., nanophytoplankton) are dominant due to strong vertical stratification and surface nutrient depletion (Li et al., 2006). In the MAB, the

86 seasonality of phytoplankton size structure is controlled by the similar mechanism as that in the
87 GoM (Pan et al., 2011). Most of the previous studies focused on the GoM and the MAB separately,
88 and a model-based integrative framework is needed to synthesize the spatiotemporal patterns and
89 to better understand the driving mechanisms.

90 Over the NAS, another understudied problem is the dynamics of organic detritus and
91 phytoplankton at the bottom and their coupling with surface productivity. Bottom detritus and
92 phytoplankton are critical energy sources for benthic organisms, including some important fishery
93 species (Townsend and Cammen, 1988; Mills et al., 2013). The abundance of detritus and
94 phytoplankton at the bottom are jointly modulated by vertical sinking from the overlying water
95 column, lateral advection, and resuspension (Cranford and Gordon, 1992; Dunne et al., 2005).
96 These physical processes, together with biogeochemical dynamics (e.g., particulate organic matter
97 decomposition), regulate the spatial distribution of phytoplankton and detritus at the bottom and
98 the energy flow from the euphotic zone to the benthos. A model-based analysis can shed light on
99 the general spatiotemporal patterns of pelagic-benthic coupling and identify the key gaps in our
100 observations.

101 Our understanding of nutrient cycling and physical-biological coupling on the NAS has
102 greatly improved over the last few decades (e.g., Malone et al., 1983; Fennel et al., 2006; Ji et al.,
103 2008b, 2008a; Townsend et al., 2014; Zhang et al., 2019). Yet some key questions regarding the
104 spatial heterogeneity of nutrient-phytoplankton dynamics in this ecosystem remain and can be
105 better addressed within an integrative modeling framework. Those questions include: 1) what is
106 the major difference between the GoM and the MAB with regard to the seasonality of
107 phytoplankton community? 2) what are the key factors controlling the spatial heterogeneity of
108 phytoplankton dynamics? 3) what are the region-specific responses of phytoplankton dynamics to

109 climate forcing on the NAS? and 4) what are the implications of spatially heterogenous
110 phytoplankton dynamics for regional pelagic and benthic production. Answering these questions
111 becomes imperative as the climate warming on the NAS seems to be accelerating (Belkin, 2009;
112 Burrows et al., 2011). The objective of this study is to establish a modeling framework to
113 synthesize observational data from various sources, and to identify the major patterns and
114 responsible drivers of the spatially variable phytoplankton seasonality. The 3-D coupled physical-
115 biological model used in this study is capable of 1) resolving latitudinal gradients and coastal-
116 shelf-slope interactions; 2) assessing sub-seasonal to interannual variabilities; 3) resolving pelagic
117 microbial food web dynamics and size-dependent functional responses to changing environmental
118 conditions. Our study focuses on the climatological patterns of nutrient and phytoplankton
119 seasonality based on a multi-year (1978-2014) model simulation described below. Analyses of
120 interannual variability will be presented in follow-up papers.
121
122 **2. Materials and Methods**
123
124 2.1 Ocean Hydrodynamic Model
125 The ocean hydrodynamic model used to force the biological model is a 3-dimensional,
126 unstructured grid, and primitive equation Finite Volume Community Ocean Model (FVCOM;
127 Chen et al., 2003). Specifically, FVCOM-Gulf of Maine Version 3 (FVCOM-GOM3) in this study
128 is a circulation model for the US Northeast Coastal Ocean Forecast System (NECOFS), which is
129 nested within the FVCOM-Global model (Chen et al., 2011). The model domain covers the NAS
130 from the Scotian Shelf to the MAB, and adjacent slope and basin regions (Fig. 1). The horizontal
131 grid resolution ranges from 10 km in the deep basins and flat shelves to 0.5 km in coastal regions

and topographically complex regions such as the shelf break, channels, and canyons. The vertical grid is discretized into 45 layers using a hybrid terrain-following coordinate (Chen et al., 2011). To support the quality of model products, FVCOM-GOM3 also assimilates mooring and ship measurements of temperature and salinity profiles using the optimal interpolation method and mooring current profiles using the nudging method (Chen et al., 2009). The physical outputs of this model have been validated through comparisons with available hydrographic observations. The model-data comparisons include 1) water elevations at tidal gauges (Chen et al., 2011; Sun et al., 2013), 2) temperature and salinity in the water column (Li et al., 2015), and 3) surface currents measured by coastal ocean dynamics application radar (CODAR) from 2000 to 2008 (Sun et al., 2016). These comparisons demonstrate that the model captures tidal- and shelf break density fronts, residual gyres, wind-driven upwelling, buoyancy-driven river plumes, the Gulf Stream-shelf interaction, and volume and mass transports entering the GoM over the Scotian Shelf from the upstream. Hourly mean outputs of this hydrodynamic model were downloaded from the data server of the University of Massachusetts Dartmouth (http://fvcom.smast.umassd.edu) to drive the marine food web model simulations in an offline coupling mode. The two successive hourly physical fields (e.g., current velocities in different directions, short wave radiation, and water temperature) are linearly interpolated to the time step of the marine food web model (i.e., 120 s). The 3-D transport equation is recalculated in two steps based on the interpolated physical fields to ensure the mass conservation of biological tracers in the food web model. In the first step, the biological variables are calculated using the advection and horizontal diffusion terms along with the biogeochemical source/sink terms. The advection terms are calculated using a second-order upwind scheme. In the second step, the vertical diffusion term is discretized and calculated using an implicit scheme following Chen et al. (2003).

155

156 2.2 Marine food web model

157 An intermediate-complexity nutrient-phytoplankton-zooplankton-detritus (NPZD) model
158 was implemented to simulate lower trophic level food web dynamics on the NAS. The nitrogen-
159 based model structure is modified from a 9-component global ecosystem model (Stock and Dunne,
160 2010) by adding a mesozooplankton group (Song et al., 2010, 2011; Fig. S1). The 10 functional
161 groups in the model include dissolved inorganic nitrogen (DIN), small phytoplankton (SP), large
162 phytoplankton (LP), small zooplankton (SZ), mesozooplankton (MZ), large zooplankton (LZ),
163 bacteria (BAC), labile small detritus (SD_L), semi-labile small detritus (SD_S), and large detritus
164 (LD). Model parameters were tuned to better fit the NAS ecosystem. The vertical settling fluxes
165 of LD, SP, and LP are resolved using a piecewise parabolic method and a weighted essentially
166 non-oscillatory (WENO) scheme. Due to the importance of resuspension in LD dynamics at the
167 bottom, one sediment layer for LD is applied to store the total amount of LD settled on the seabed.
168 The remineralization rate of LD in the sediment layer is specified as zero. The resuspension flux
169 of LD (E_{LD}) is estimated based on current-induced bottom shear stress following Ariathurai and
170 Arulanandan (1978), and E_{LD} can directly influence the concentration of LD in the bottom water
171 layer. Zooplankton grazing terms in the model utilize Holling type II formulation if only one type
172 of prey is available. When multiple types of prey exist, the switching response of grazing is
173 included (Gentleman et al., 2003; Stock et al., 2008; Stock and Dunne, 2010). The fractions of MZ
174 and LZ consumed by higher predators (HP) are based on their relative abundance and HP grazing
175 rate following the switching response of grazing as well (Stock and Dunne, 2010). To simplify
176 model processes, the atmospheric deposition of nutrients at the surface and denitrification
177 processes at the bottom boundary are not considered, although some prior studies have suggested

178 those processes might be important in nitrogen cycling during certain time periods (Fennel et al.,
179 2008; Friedrichs et al., 2019).

180 The focus of this study is phytoplankton dynamics and size composition, so we only show
181 the growth rate equations for SP and LP. The role of zooplankton in the NAS ecosystem is beyond
182 the scope of this paper and will be assessed in our follow-up studies. Readers are referred to Geider
183 et al. (1997), Stock and Dunne (2010) and Song et al. (2011) for more details regarding the model's
184 structure and equations. The phytoplankton growth rates of SP (μ_{SP}) and LP (μ_{LP}) are limited by
185 temperature ($f(T)$), nutrient concentration ($g(N)$), and light availability for photosynthesis ($h(I)$),

186 $$\mu_{SP(LP)} = \frac{\mu_{SP(LP),max}}{1+\zeta_{SP(LP)}} \cdot f(T) \cdot g(N) \cdot h(I) - meta_{SP(LP)} \cdot f(T) \quad (1)$$

187 $$f(T) = (Q_{10,SP(LP)})^{\frac{T-20}{10}} \quad (2)$$

188 $$g(N) = \frac{N}{K_{N,SP(LP)}+N} \quad (3)$$

189 $$h(I) = 1 - \exp\left(-\frac{\alpha_{SP(LP)} \cdot I \cdot \theta_{SP(LP)}}{\mu_{SP(LP),max} \cdot f(T) \cdot g(N)}\right) \quad (4)$$

190 Here $\mu_{SP(LP),max}$ and $meta_{SP(LP)}$ are maximum nutrient-saturated growth rate and basal
191 metabolism rate of phytoplankton at the reference temperature (20°C), respectively. $Q_{10,SP(LP)}$ is
192 phytoplankton temperature dependence coefficient. $K_{N,SP(LP)}$ represents half saturation coefficient
193 for nutrient-limited growth. *I* is the incoming shortwave radiation flux for photosynthesis at the
194 center of each grid. $\alpha_{SP(LP)}$ is the initial slope of the photosynthesis-irradiance (P-I) curve.
195 $\zeta_{SP(LP)}$ is the fraction of biosynthesis cost. Chlorophyll to carbon ratio, $\theta_{SP(LP)}$, is defined following
196 Geider et al. (1997). All model parameters mentioned above are described in Table S1. It is worth
197 noting that silicate is another important limiting nutrient for LP (i.e., diatom) in our study region
198 (e.g., Townsend et al., 2006, 2010). Given roughly equal proportions of nitrate and silicate taken

199 up by diatoms and relatively lower concentrations of silicate than nitrate in the GoM, silicate is
200 depleted earlier and limits the growth of diatoms in the center of the GoM (Townsend et al., 2006).
201 In coastal regions, however, the depletion of nitrate during the spring bloom limits the growth of
202 phytoplankton due to silicate-rich terrestrial discharge (Schoudel, 1996). The model implemented
203 for this study follows our earlier model configuration without silicate cycle (Stock and Dunne,
204 2010; Song et al., 2011). This caveat needs to be taken into consideration when interpreting the
205 model results, especially for the deep central GoM region.
206
207 2.3 Observational data sets
208 To assess our model's hindcast skills in reproducing phytoplankton climatology and
209 seasonality, we compiled both ship-based measurements and satellite data for model-observation
210 comparison. Historical in-situ chlorophyll measurements of small-sized nanoplankton (2-20 μm)
211 and large-sized netplankton (20-300 μm) were retrieved from a total of 182 cruises (August 1976
212 to January 1988) during Marine Resources Monitoring, Assessment & Prediction (MARMAP)
213 Program of the National Oceanic and Atmospheric Administration (NOAA). The details of sample
214 acquisition and laboratory processing procedures were described in O'Reilly and Zetlin (1998).
215 Given MARMAP's monthly to seasonal sampling frequencies and strong mixing over the top 10
216 m (Tian et al., 2014; Li et al., 2015), we computed bimonthly climatology (January-February,
217 March-April, May-June, July-August, September-October, and November-December) of large vs.
218 small phytoplankton size ratio by averaging observed values every 0.5° grid between 0 and 10 m
219 depths. In addition, the bimonthly chlorophyll composites of GlobColour merged satellite products
220 (http://www.globcolour.info) from 1998 to 2014 were interpolated to the model grid and compared
221 with the simulated surface chlorophyll climatology to demonstrate the bimonthly patterns of model

results (Maritorena et al., 2010). It is worth noting that this bimonthly comparison between model results and satellite images was not for the assessment of detailed bloom timing due to the coarse temporal resolution. An EOF analysis with a higher temporal resolution (8-day composite) was conducted to evaluate more detailed timing variability patterns across the entire model domain. Field observations of nitrogen (NO_3+NO_2) and chlorophyll were extracted from the Gulf of Maine Region Nutrient and Hydrographic Database (http://grampus.umeoce.maine.edu/nutrients), a combination of several global and regional datasets (Rebuck and Townsend, 2014).

2.4 Sensitivity Tests

The response of phytoplankton growth rate to temperature is crucial in simulating marine primary productivity, and its parameterization directly impacts the model's capacity in reproducing ocean ecosystem dynamics under the rapid global climate change. Our model utilize a Q_{10} relationship to represent the response of phytoplankton growth rate to temperature variation (see equation 2). The maximum growth rate of phytoplankton increases (decreases) with the elevation of $Q_{10,SP(LP)}$ above (below) the reference temperature (20 ºC in this study) and vice versa (Fig. S2). Q_{10} was specified as 2.0 in our benchmark run following previous studies (Ji et al., 2008b; Stock and Dunne, 2010; Song et al., 2011). However, estimations of Q_{10} based on measurements suggested that many factors (e.g., species, physiological changes, temperature interval, genotypic difference) could cause significant deviations from 2.0 (Eppley, 1972; Sherman et al., 2016). Here we increased/decreased $Q_{10,SP(LP)}$ by 0.3 and 0.6, respectively, and conducted

242 one-year simulations in 1978 to examine its importance in the seasonality of phytoplankton
243 dynamics over the NAS.
244
245 **3 Results**
246
247 3.1 Nitrogen dynamics in the GoM and the MAB
248 We compared simulated monthly-averaged nitrogen concentration over the top 10 m with
249 observations in the GoM and the MAB (see Fig. S3 for locations). Our model reasonably
250 reproduced the temporal variability of surface nitrogen, i.e., high in winter (> 5 mmol/m^3) and low
251 in summer (< 2 mmol/m^3) (Fig. S4). The time series of simulated nitrogen was well correlated
252 with measurements in the GoM (r=0.85; RMSE=1.49) and the MAB (r=0.68; RMSE=1.86),
253 indicating the robust performance of our model in reproducing the seasonality of surface nitrogen
254 on the NAS (Fig. S4). The simulated deep nitrogen below 100 m was also comparable to the field
255 observed concentrations without a strong seasonality (Fig. S5).
256 To better demonstrate the seasonality of nitrogen concentration, the annual cycle of
257 monthly mean temperature versus surface nitrogen concentration is shown in Fig. 2. The
258 comparison between model and observations suggested that our model well captured the seasonal
259 variation of nitrogen, which was strongly linked to thermal regime shifts among different seasons.
260 The annual cycle was similar in the GoM and the MAB: nitrogen reached the highest level from
261 January to March and the lowest level from May to September. The most dominant nitrogen
262 difference between the GoM and the MAB was found in winter, during which nitrogen
263 concentration in the MAB was about 4 mmol/m^3 lower than that in the GoM. In the summer season,

264 the nitrogen concentration difference between the two regions was less than ~ 1 mmol/m^3, while
265 the water temperature differed by up to 8°C.
266
267 3.2 Spatiotemporal variability of surface chlorophyll
268 We compared the bimonthly GlobColour-derived chlorophyll composites with simulation
269 results (chlorophyll from both phytoplankton size classes combined) to assess the model's
270 performance in reproducing the surface phytoplankton dynamics (Fig. 3). Over the entire study
271 area, the chlorophyll concentration was higher along the coast due to vertical mixing in shallow
272 areas and decreased gradually offshore. Our simulated chlorophyll concentration in coastal regions
273 was overall lower than the satellite results (Fig. 3). The offshore chlorophyll hotspot on Georges
274 Bank had concentrations exceeding 1 mg/m^3 year-round. Shallow water depth, strong tidal mixing,
275 and offshore nutrient supply jointly contributed to the formation of this productivity hotspot (Hu
276 et al., 2008; Ji et al., 2008a). The seasonality of chlorophyll was well reproduced in our simulation:
277 the spring bloom was found in March and April when the chlorophyll concentration reached more
278 than 1 mg/m^3 on the shelf in both the GoM and the MAB (Figs. 3b and 3h). The appearance of
279 spring bloom corresponded with water warming, increased light for photosynthesis, stratification,
280 and high surface nitrogen concentration (> 1 mmol/m^3), and the remarkable decrease of nitrogen
281 in March and April was caused by rapid phytoplankton growth and weakened nutrient
282 replenishment associated with stratification (Figs. 2 and 4a). From May to August, the decreased
283 chlorophyll over the NAS resulted from nitrogen limitation and reduced chlorophyll-to-carbon
284 ratio associated with high light levels, despite higher temperature and favorable light condition for
285 phytoplankton growth (Figs. 3c, 3d, 3i, 3j and 4b). The secondary bloom took place in September
286 and October due to nitrogen replenishment associated with enhanced vertical mixing (Figs. 2, 3e,

287 3k and 4a). From November to February, high nitrogen concentration (GoM: 6–9 mmol/m^3; MAB:
288 2–4 mmol/m^3), low water temperature (GoM: 4–8°C; MAB: 5–11°C), and low light levels
289 indicated the NAS shifted to a light- and temperature-limited ecosystem (Figs. 2, 3a, 3f, 3g, 3l and
290 4b).

291 We further evaluated the model's performance by conducting Empirical Orthogonal
292 Function (EOF) decomposition to the 8-day composite of chlorophyll climatology based on both
293 model results and the GlobColour data (Fig. 5). Prior to the EOF decomposition, the climatology
294 was normalized by subtracting its temporal mean and dividing the standard deviation of each
295 model node following Yoder et al. (2002). The first modes of both model (62.9% of the total
296 variance) and GlobColour (48.8% of the total variance) suggested that chlorophyll over most
297 regions varied synchronously (Figs. 5a and 5b), although the negative pattern in the eastern GoM
298 GlobColour data was not seen in our model. The time series of the first mode illustrated the
299 canonical seasonality of chlorophyll with a primary bloom in winter-spring and a secondary bloom
300 in fall (Figs. 5a and 5b). In the first mode, the simulated secondary bloom was about one month
301 earlier than the satellite data. The discrepancy in the timing of secondary bloom could be caused
302 by the overestimated surface nitrogen concentration in September in the GoM (observation: 1.2
303 mmol/m^3; model: 1.8 mmol/m^3) and the MAB (observation: 0.4 mmol/m^3; model: 0.7 mmol/m^3)
304 (Fig. 2). The second mode accounted for 13.5% and 15.3% of the total variance in model results
305 and GlobColour data, respectively. The corresponding spatial patterns showed that chlorophyll in
306 the GoM and the MAB were out of phase: a negative pattern was prevalent over the entire GoM,
307 while a positive pattern dominated the MAB (Figs. 5c and 5d). The boundary of these two opposite
308 patterns located over the Nantucket Shoals along the 70 °W meridian. The time series of the second

309 mode demonstrated winter maxima and summer minima in the MAB, while the opposite temporal
310 variation was found in the GoM (Figs. 5c and 5d).

311 To investigate what was responsible for the spatial heterogeneity of surface chlorophyll on
312 the NAS, we estimated water temperature and nitrogen climatology at the surface using the 8-day
313 composite of our model in the GoM and the MAB, respectively. It is noteworthy that the surface
314 photosynthetic available radiation (PAR) contributes little to the spatial heterogeneity of
315 chlorophyll between the GoM and the MAB, especially when compared with the differences of
316 temperature and nutrient in these two regions (Figs. 4b, 6a and 6b). Water temperature and nitrogen
317 concentration were out of phase by 6 months in both regions: temperature peaked in summer and
318 minimized in winter, whereas nitrogen concentration was low in summer and high in winter (Figs.
319 6a and 6b). Based on our modeled water temperature and nitrogen concentration, we derived the
320 annual cycle of $f(T)$ and $g(N)$ for SP and LP in different regions to quantitatively estimate the
321 relative importance of nutrient and temperature in phytoplankton growth (see equations 2 and 3).
322 In our model, $g(N)$ and $f(T)$ jointly limited the growth of phytoplankton, and Liebig's law of
323 minimum was not applied in this study. In the GoM, the $g(N)$ of SP was around 0.9 with very
324 limited temporal variation. The $f(T)$ of SP in the GoM, however, shifted from 0.38 in winter to
325 0.81 in summer, and it was lower than $g(N)$ year-round, implying the growth of SP in the GoM
326 was more limited by temperature than by nitrogen (blue line in Fig. 6c). Owing to lower nitrogen
327 concentration and higher temperature in the MAB (Figs. 6a and 6b), the impact of limited nitrogen
328 to SP growth surpassed that of temperature ($g(N) < f(T)$) from late spring to the end of summer
329 (red line in Fig. 6c). Since we employed the same Q_{10} but higher half-saturation coefficient (K_n)
330 for LP, the $f(T)$ of SP and LP were identical, but the $g(N)$ of LP was lower than that of SP.
331 Compared with SP, the growth of LP was more sensitive to the variation of nitrogen, especially in

summer when nitrogen concentration was less than 2 mmol/m^3 (Figs. 6b and 6d). LP's $g(N)$ in the GoM ranged from 0.56 to 0.91, which was lower than its $f(T)$ from late spring to late summer (blue line in Fig. 6d). In the MAB, the duration of $f(T) > g(N)$ was even longer starting from mid-spring until early fall (red line in Fig. 6d). In general, the intrinsic growth rate of phytoplankton in the GoM was more limited by temperature than by nitrogen, while relatively lower nitrogen concentration and higher water temperature in the MAB contributed to stronger nutrient limitation on phytoplankton growth. Compared with the second mode of chlorophyll EOF analysis (Figs. 5c and 5d), the seasonality of temperature and nitrogen and their limiting effects roughly matched the second mode of EOF analysis in the GoM and the MAB, respectively. In the GoM, low temperature strongly limited the growth of phytoplankton in the cold season, resulting in the shift of two blooms in the canonical seasonality of phytoplankton (the first mode of EOF analysis) towards the warm season with a delayed spring bloom and an advanced fall bloom. In the MAB, the increased importance of nutrient limitation in the warm season and relatively high temperature in late fall and winter shifted the bloom timings towards the opposite direction (an earlier primary bloom in winter and a later secondary bloom in fall).

3.3 The seasonality of phytoplankton size structure

Both model results and the MARMAP dataset illustrated a strong seasonality of phytoplankton size structure over the NAS (Fig. 7). In January and February, LP was abundant in coastal regions (LP fraction > 70%), while SP dominated offshore and the center of the GoM (Figs. 7a and 7g). In March and April, LP became dominant on the NAS, reflecting the importance of diatoms in the winter-spring phytoplankton bloom (Figs. 7b and 7h). Subsequently, the dominant phytoplankton type shifted from LP to SP rapidly over the entire shelf until the end of August,

when LP only dominated sporadically along the coast of the GoM and over Georges Bank (Figs. 7c, 7d, 7i and 7j). From September to December, the percentage of LP increased moderately with minor changes in spatial distribution pattern (Figs. 7e, 7f, 7k and 7l).

We further compared the simulated monthly LP fraction ($\frac{LP}{LP+SP} \times 100\%$) with the observations in the GoM and the MAB, respectively (Fig. 8). High correlation coefficients (GoM: $r = 0.83$; MAB: $r = 0.90$) suggested our simulated phytoplankton size structure matched that of the observations, although the LP fraction appeared to be overestimated in the GoM throughout the year (Fig. 8). The LP fraction in the GoM increased gradually from January to April, and the peak value (~60%) was followed by a sharp decrease until July (Fig. 8a). After that, the LP fraction increased slightly and fluctuated around 30% until the end of the year. In the MAB, the temporal variation of LP fraction was overall similar to that in the GoM (high in the cold season and low in the warm season), while both the peak and trough of LP fraction appeared about one month in advance (Fig. 8b).

3.4 EOF results of bottom LD and chlorophyll

To examine the links between pelagic production and exported organic materials reaching the seafloor, we applied EOF analysis to 8-day composites of chlorophyll and LD climatology in the bottom layer to reveal their spatiotemporal patterns (Fig. 9). For bottom chlorophyll, the spatial patterns of the first two modes were very similar to those of surface chlorophyll: positive pattern dominated the entire shelf in the first mode except for the deep central GoM, and opposite patterns between the GoM and the MAB were found in the second mode (Figs. 9a and 9c). For bottom chlorophyll, the first EOF mode did not have a fall peak. The first two modes of bottom LD, however, had very different spatiotemporal patterns compared with the corresponding modes of

chlorophyll (Figs. 9b and 9d). The GoM and the MAB had opposite patterns in the first mode of bottom LD, and the corresponding time series had a sinusoidal annual cycle (Fig. 9b). The spatial heterogeneity in the second mode of bottom LD was even greater over the NAS (Fig. 9d).

3.5 Thermal sensitivity of phytoplankton dynamics

To investigate the sensitivity of phytoplankton dynamics to temperature and to explore how Q_{10} parameterizations can affect modeled phytoplankton's seasonality, we compared the time series of chlorophyll concentration in the top 10 m between the benchmark run and sensitivity test runs (Fig. 10). In the GoM, the major discrepancies among different cases were detected during both the spring and fall blooms, while minor difference in chlorophyll concentrations occurred during the rest of the year (Fig. 10a). In the MAB, only the spring bloom was sensitive to changes in Q_{10} (Fig. 10b). To quantitatively estimate the impacts of Q_{10} on phytoplankton dynamics, we derived the timing and magnitude of blooms in the GoM and the MAB following Ji et al. (2007). As Q_{10} increased from 1.4 to 2.6, the peak of the spring bloom in the GoM was delayed from mid-March to mid-May with a remarkable magnitude decrease from 6.5 mg/m^3 to 1.8 mg/m^3 (Figs. 10c and 10d). The spring bloom magnitude declined with higher Q_{10} in the GoM because climatological mean temperature in the GoM was always lower than the reference temperature (20°C; Fig. 6a), below which higher Q_{10} value corresponded to lower phytoplankton growth rate in the Q_{10} model (Fig. S2). In the MAB, the timing of the spring bloom was insensitive to the variation of Q_{10}, while its magnitude decreased markedly from 5.6 to 1.8 mg/m^3 as Q_{10} increased (Figs. 10c and 10d). The timing of the fall bloom in the two areas advanced about 15 days with slightly reduced magnitude as Q_{10} increased from 1.4 to 2.6 (Figs. 10c and 10d). Overall, a lower Q_{10} value contributed to an earlier spring bloom and a later fall bloom with enhanced magnitude,

401 and phytoplankton dynamics in the GoM was more sensitive to Q_{10} variations than that in the
402 MAB.
403
404 **4 Discussion**
405
406 4.1 Spatial heterogeneity of thermohaline structure and phytoplankton dynamics on the NAS
407 In our study region, the GoM and the MAB have different thermohaline structures (Li et
408 al., 2015). In the MAB, water temperature is higher than that in the GoM due to the combination
409 of strong surface heating, exchange with warm slope water, and the absence of direct cold water
410 inflow from subpolar regions (Loder, 1998); The nearshore salinity in both regions is significantly
411 influenced by terrestrial freshwater discharge, while low-salinity water inflow from higher latitude
412 further enhances freshening in the GoM during winter-spring season (Mountain and Manning,
413 1994). The difference of thermohaline structures between the GoM and the MAB results in a
414 distinct annual cycle of stratification in these two regions: earlier and stronger stratification in the
415 MAB is thermally-dominated through a large portion of the year, whereas haline control
416 strengthens in the GoM (Li et al., 2015). Many studies have confirmed that surface nutrient
417 replenishment is strongly correlated with mixing (e.g., Townsend, 1998; Townsend et al., 2010).
418 As stated in Section 3.2, different surface nutrient regimes and water temperature between the
419 GoM and the MAB are responsible for the spatial heterogeneity of phytoplankton dynamics
420 between the two regions: in the GoM, relatively high nutrient concentration due to strong mixing
421 and low water temperature result in weaker limitation of nutrient but stronger limitation of
422 temperature for phytoplankton growth. On the other hand, stratification-induced lower nutrient
423 supply and warmer water in the surface mixed layer of the MAB contribute to more significant

nutrient limitation. Chlorophyll concentration in the GoM reaches a maximum in spring, while the primary bloom on the MAB shelf occurs earlier in winter. The spatial heterogeneity of phytoplankton dynamics might also exist between the eastern GoM and western GoM (Fig. 5b). Compared with surface chlorophyll observations, the spring bloom cannot be detected in the GlobColour satellite data in the eastern GoM (Figs. S6 and S7), and this bias contributes to the opposite pattern in the first EOF mode of the satellite data (Fig. 5b). The quality of GlobColour data in the eastern GoM might be compromised by colored dissolved organic matter and resuspended sediment (Butman et al., 2014; Balch et al., 2016). The spring bloom in the eastern GoM is reproduced in our model results, whereas the simulated spring bloom happens earlier with relatively low magnitude compared to field measurements (Figs. S6 and S7). Therefore, the difference in the eastern GoM between model and satellite in the first mode of EOF analysis can be ascribed to the errors in both simulation results and satellite products.

In the cross-shelf direction, both model and satellite images demonstrate that chlorophyll concentration in the GoM decreases from shallow coastal regions to deep basins, although the cross-shore gradient of model results is relatively low because of the underestimation of simulated chlorophyll nearshore (Fig. 3). The discrepancy can be a result of overestimated chlorophyll concentration in satellite data due to high colored dissolved organic matter and sediment concentrations nearshore, or underestimated chlorophyll concentration in simulation results due to the improperly resolved phytoplankton-grazer linkages and the absence of large, chain-forming coastal large phytoplankton in our model (Hyde et al., 2007; Van Oostende et al., 2018). Over the MAB, however, the cross-shelf gradient of chlorophyll is more complicated due to strong interactions between shelf and slope waters (Malone et al., 1983). The canonical viewpoint suggests a dramatic decrease of chlorophyll concentration from the MAB shelf to slope (Malone

et al., 1983; Yoder et al., 2001), whereas high chlorophyll concentration on the shelf break has been recorded by both satellite data and field measurements (Ryan et al., 1999; Mouw and Yoder, 2005). Unlike the winter bloom over the MAB shelf, the chlorophyll bloom over the shelf break regions occurs in spring with lower magnitudes (Xu et al., 2011). The cross frontal water exchange, due to many factors (e.g., frontal instability, wind, warm-core rings, and shelf break upwelling), contributes to nutrient delivery to the euphotic zone and stimulates chlorophyll enhancement in the shelf break region (Ryan et al., 1999). This offshore bloom can be found in our simulation results as well (Figs. 3i, 3j and 3k), yet such a feature does not exist in satellite climatology (Figs. 3c, 3d and 3e). The discrepancy between model and satellite data can be attributed to the model underestimation of zooplankton grazing pressure (Zhang et al., 2013), but more studies are needed to explore the underlying mechanisms.

The spatial heterogeneity of phytoplankton size structure between the GoM and the MAB is strongly related to diatom blooms: the diatom blooms in the GoM and the MAB occur in winter-spring, and the bloom asynchrony results in phytoplankton size structure difference between the two regions (Fig. 8). Unlike the winter diatom bloom on the MAB shelf, the bloom over the MAB shelf break occurs in spring and is dominated by small phytoplankton (Ryan et al., 1999). Consequently, the seasonality of phytoplankton size structure over the MAB shelf break is different from the rest of the NAS.

The increase of sea surface temperature in the GoM is reported to be faster than most of the global ocean (Pershing et al., 2015), and future projections suggest this rapid warming will continue (Loder et al., 2015). As suggested by this study, water temperature and nutrient level at the surface are responsible for the spatial heterogeneity of phytoplankton dynamics between the GoM and the MAB. It then begs the question of will phytoplankton dynamics in the GoM become

more similar to that in the MAB as the GoM warms in the upcoming decades. If the temperature effect on growth rate is the dominant factor regulating the abundance of phytoplankton, the increasing thermal regime similarities between the GoM and the MAB can potentially reduce the spatial heterogeneity of phytoplankton seasonality (Shearman and Lentz, 2010). However, this direct temperature effect can be confounded by the surface nutrient dynamics regulated by stratification, which is more thermally regulated in the MAB compared to the haline-controlled GoM during the winter-spring bloom season (Li et al., 2015). Both satellite and model results indicate the importance of freshening in winter-spring bloom timing and magnitude (Ji et al., 2007, 2008b). Besides, the increasing similarity in the surface thermal regimes between the GoM and the MAB might not result in similar vertical stratification patterns. Warming over the NAS can be ascribed to both surface heating associated with atmospheric warming and lateral advection at depth, which have different impacts on the intensity of stratification (Shearman and Lentz, 2010; Chen et al., 2014). Consequently, vertical stratification and related surface nutrient-phytoplankton dynamics in the GoM and the MAB can still be distinctive even as their surface thermal regimes become similar under rapid warming.

4.2 Impact of warming on phytoplankton dynamics on the NAS

In the context of global climate change, surface water temperature in the NAS ecosystem has been increased markedly over the last several decades, with a warming rate of ~0.26 °C/yr starting from the early 21st century (Belkin, 2009; Shearman and Lentz, 2010; Burrows et al., 2011; Mills et al., 2013). However, a comprehensive understanding of phytoplankton response to rapid warming remains challenging due to the complex physical-biogeochemical interactions and tight coupling between different trophic levels. As ambient water temperature increases, the growth of

493 phytoplankton becomes faster due to the thermal adaptation (Eppley, 1972; Staehr and Birkeland,
494 2006), and the growth rate becomes more sensitive to temperature variations (Fig. S2). By contrast,
495 surface heating-induced stratification reduces surface phytoplankton growth by constraining
496 nutrient replenishment (Figs. 2 and 3; Thomas et al., 2003; Song et al., 2011). Previous studies
497 have suggested low nutrient availability has a strong effect on phytoplankton growth (e.g., Staehr
498 and Birkeland, 2006). In addition, temperature modulates nutrient dynamics via not only
499 stratification, but also biogeochemical processes. Laurent et al. (2016) applied temperature-
500 dependent remineralization rate of particulate organic matter in the diagenetic model and found
501 that the nitrogen dynamics were very sensitive to water temperature. The rates of many other
502 nitrogen pathways (e.g., nitrification, nitrogen fixation) are also strongly correlated with water
503 temperature (Damashek and Francis, 2018), implying the importance of temperature in nitrogen
504 cycling and its potential impacts on phytoplankton growth.

505 Climate-related warming also regulates the growth of phytoplankton ($\mu_{SP(LP)}$ in equation
506 1) via changing phytoplankton temperature dependence coefficient Q_{10}, which represents the
507 thermal responses of the community and varies greatly with the shift of phytoplankton community
508 composition (Staehr and Birkeland, 2006). Physical conditions such as turbulence and temperature,
509 as well as the nutrient regimes, are the primary factors affecting phytoplankton composition: small
510 phytoplankton, such as dinoflagellates, become dominant when the water column is stable and
511 oligotrophic, while large phytoplankton species (e.g., diatoms) are more common in less stratified
512 and nutrient-rich environments (Margalef, 1978; Pershing and Stamieszkin, 2020). As rapid
513 warming continues over the NAS, longer and stronger thermal stratification will favor the
514 dominance of small phytoplankton (Thomas et al., 2017). Due to the wide range of Q_{10} between
515 phytoplankton species, it is reasonable to speculate that the shift of phytoplankton community

516 composition might affect the value of community Q_{10}. Moreover, the thermal adaptation of
517 phytoplankton alters their physiological features and consequently the Q_{10} values, and such
518 response is usually species-specific (Staehr and Birkeland, 2006). Sherman et al. (2016) estimated
519 the Q_{10} value based on a global database of field measurements and found the optimum apparent
520 Q_{10} was around 1.5, which was lower than the value (2.0) in our study. Our Q_{10} sensitivity tests
521 with low Q_{10} values (tests 1 and 2), however, overestimated chlorophyll concentration
522 dramatically during blooms (Fig. 10), implying the Q_{10} in the NAS might greatly deviate from the
523 global mean value. Given the importance of Q_{10} parameterization in simulating phytoplankton
524 dynamics (Fig. 10), the variation of community Q_{10} may modulate phytoplankton dynamics in the
525 entire NAS ecosystem.

526 From a top-down control perspective, climate-related warming manipulates phytoplankton
527 abundance via changing zooplankton dynamics. Our EOF results of surface mesozooplankton are
528 similar to that of chlorophyll, implying a tight coupling between zooplankton and phytoplankton
529 (Figs. 5 and S8). The ramifications of climate-induced warming for phytoplankton dynamics on
530 the NAS propagate through the food web in both bottom-up and top-down directions. Due to the
531 simplified structures of most 3-D biogeochemical models, they can only partially resolve the
532 influence of temperature on marine ecosystems. Future models need to better resolve thermal
533 responses of important physical-biogeochemical processes in order to improve the model
534 projections of future climate scenarios.

535

536 4.3 Benthic-pelagic coupling on the NAS

537 The NAS supports some of the commercially important benthic species (e.g., groundfish,
538 sea scallop, and lobster; Pershing and Stamieszkin, 2020), and their high production is mainly

539 fueled by the sedimentation of surface organic matter (Griffiths et al., 2017). Thus, understanding
540 benthic-pelagic coupling in our study area can help us gain more insight in developing adaptive
541 fishery management strategies under a rapid changing climate. As stated in section 3.4, the
542 seasonality of bottom chlorophyll modulated by the settling of surface-subsurface phytoplankton,
543 deep production and chlorophyll to carbon ratio is overall analogous to that in the surface layer
544 over the entire study area, while the seasonality of bottom chlorophyll in the deep basins of the
545 GoM is very weak. The decoupling between the surface and the bottom chlorophyll concentrations
546 in the deep basins is probably bathymetry–driven: the sinking of phytoplankton from the surface
547 to the bottom takes longer time over the deep basins, allowing a significant loss of phytoplankton
548 due to zooplankton grazing, respiration, aggregation, exudation, and viral lysis, thus weakening
549 the seasonality of bottom chlorophyll and benthic-pelagic coupling. Additionally, there is no
550 detectable bottom chlorophyll increase in fall, possibly due to the slow settling of small
551 phytoplankton that dominate the fall bloom at the surface (Figs. 7 and 8). The enhancement of
552 vertical mixing in fall might further contribute to the decrease of phytoplankton settling flux on
553 the NAS (Arin et al., 2002; Ross, 2006).

554 For LD at the bottom, its opposite spatial pattern in the first mode could be explained by
555 vertical settling and production in the euphotic layer: in the GoM, relatively low productivity
556 throughout the water column (Fig. S9) and strong vertical mixing in the cold season result in the
557 reduced LD settling flux to the bottom and the increase of LD upward flux from the bottom to the
558 overlying water (Arin et al., 2002; Ross, 2006). In the warm season, stratification limits the LD
559 mixing from the bottom to the surface, and the enhanced surface production can increase the
560 settling flux of LD from the euphotic layer to the bottom (Fig. S9). On the inner shelf of the MAB,
561 both strong stratification in the warm season and shallow water depth shorten the duration of LD

settling from the euphotic layer to the bottom and contribute to the coupling between surface production and bottom LD concentration: higher surface production and bottom LD concentration are found in winter and spring, while lower values appear in summer (Figs. 5 and 9). The opposite pattern on the outer shelf of the MAB might result from the interactions with slope water (Fig. 9b; Townsend et al., 2006; Xu et al., 2011). The spatial heterogeneity in the second mode is likely related to LD resuspension, which is determined by local current fields in our model. On the NAS, LD resuspension due to tidal currents has strong spatiotemporal variations. In the GoM, the intensity of current-induced resuspension decreases gradually from coastal regions to deep basins (Butman et al., 2014). In the MAB, both observations and model results suggest energetic winter storms and hurricanes are the major driving forces of strong resuspension, and the contribution of tidal currents becomes very limited (Miles et al., 2015). Since LD is an important food source for benthic organisms, the prominent difference between surface productivity and bottom LD suggests that the pelagic and benthic layers are at least partially uncoupled. It is worth noting that our model, like many 3D biogeochemical models, cannot comprehensively resolve LD resuspension and other benthic-pelagic coupling processes, whose importance in organic matter distribution and nutrient cycling has been emphasized in recent numerical studies (e.g., Laurent et al., 2016; Moriarty et al., 2018). Future modeling efforts should include the dynamics of benthic-pelagic coupling for the NAS ecosystem.

4.4 Model limitations and future work

Although our model results provide valuable insights into the seasonality of phytoplankton dynamics in the NAS and driving mechanisms for its spatial heterogeneity, this model has some limitations and warrants further improvements. Firstly, our model considers nitrogen as the only

585 limiting nutrient, even though silicate could be another important nutrient (Townsend et al., 2006).
586 Given the distinct silicate sources between coastal and offshore regions, silicate dynamics might
587 potentially regulate phytoplankton community heterogeneity, especially during spring blooms
588 when diatoms are dominant over the entire shelf. Phosphate is not usually treated as the limiting
589 nutrient in the NAS, while recent field measurements suggest its importance in summer (Townsend
590 et al., 2014). Future modeling development needs to carefully assess the role of other potentially
591 limiting nutrients.

592 Global eco-evolutionary model results suggest the thermal adaptation can mitigate the loss
593 of phytoplankton diversity owing to its rapid reproduction (Thomas et al., 2012). However,
594 designing a parameterization scheme to well represent phytoplankton adaptation to rapid warming
595 is still challenging due to the lack of thermal adaptation information in a variety of taxa.
596 Considering the distinct responses to warming between different phytoplankton species (Staehr
597 and Birkeland, 2006), characterizing thermal adaptation of the dominant species in the NAS
598 system becomes essential in climate projection of future ecosystem responses.

599 Many field measurements and laboratory cultures indicate phytoplankton sinking velocity
600 varies dramatically, and it is influenced by many factors such as nutrient availability,
601 morphological features of cells, and physical environments (Bienfang et al., 1983). Besides, some
602 species of large diatoms undergo bursts of rapid sinking (sinking velocity increases from almost
603 zero to 0.2 mm/s in several seconds), and such behavior benefits the growth of diatom by
604 enhancing nutrient flux to cell surface (Gemmell et al., 2016). All these findings suggest the
605 constant sinking velocity scheme employed in most biological models might not be able to
606 adequately resolve phytoplankton vertical settling flux, and such an oversimplification can
607 introduce substantial uncertainties in simulating primary production, carbon sequestration, and

608 benthic-pelagic coupling (Griffiths et al., 2017). In future studies, a dynamic phytoplankton
609 sinking velocity scheme should be developed and applied to biological models to better represent
610 phytoplankton settling process.
611
612 **5 Conclusions**
613
614 A 3-D physical-biogeochemical model was applied in the NAS ecosystem to investigate
615 the seasonality of phytoplankton dynamics and the underlying mechanisms modulating its spatial
616 heterogeneity. The spatial heterogeneity on the NAS resulted from the joint influences of nutrient
617 availability and temperature-related physiology: a strong impact of nutrient limitation in the MAB
618 lead to an earlier winter bloom and a later fall bloom, while a delayed spring bloom and an
619 advanced fall bloom in the GoM could be attributed to the dominance of temperature limiting
620 effect. Chlorophyll concentrations at the surface and bottom were coupled, whereas stratification
621 and mixing, interaction with slope water, and resuspension attributed to the decoupling between
622 bottom detritus and surface productivity. Given the importance of phytoplankton in the marine
623 food web, its spatial heterogeneity over the NAS could impact trophic connections between
624 phytoplankton and zooplankton. The differences in thermohaline structure and warming
625 mechanisms between the GoM and the MAB contributed to the distinct responses of phytoplankton
626 abundance to climate-related warming in the two regions. Most biogeochemical models could only
627 partially reproduce the impact of warming on the marine ecosystem due to their simplified
628 structures. To better simulate the impact of rapid warming on phytoplankton dynamics on the NAS,

parameterizations of numerous temperature-related processes (e.g., stratification, nutrient cycling, and zooplankton grazing) should be improved in the future.

Data Availability

The original marine food web model data underlying this article will be shared on reasonable request to the corresponding author. The processed bimonthly MARMAP phytoplankton size structure data with 0.5° resolution in our study region is available at http://ulysse2.whoi.edu:8080/thredds/catalog/data/zzang/MARMAP_bimonth/catalog.html.

Acknowledgements

This study was supported by NOAA Coastal and Ocean Climate Application (COCA) Program (NA17OAR4310273) and NSF Northeast US Shelf - Long-Term Ecological Research (NES-LTER) Program (OCE-1655686). Computational support was provided by HPC system (cluster Poseidon) at WHOI. The model results and processed observation data are stored in WHOI HPC system. Kimberly Hyde and Chris Melrose provided the original MARMAP size-fractionated phytoplankton data. This study greatly benefited from discussions with the NES-LTER team members and Yun Li at University of Delaware. Constructive comments and suggestions from two anonymous reviewers and editor are much appreciated.

References

Ariathurai, R., Arulanandan, K., 1978. Erosion rates of cohesive soils. J. Hydraul. Div. 104, 279–283.

Arin, L., Marrasé, C., Maar, M., Peters, F., Sala, M.-M., Alcaraz, M., 2002. Combined effects of nutrients and small-scale turbulence in a microcosm experiment. I. Dynamics and size distribution of osmotrophic plankton. Aquat. Microb. Ecol. 29, 51–61.

Balch, W., Huntington, T., Aiken, G., Drapeau, D., Bowler, B., Lubelczyk, L., Butler, K., 2016.

Toward a quantitative and empirical dissolved organic carbon budget for the Gulf of Maine, a semienclosed shelf sea. Global Biogeochem. Cycles 30, 268–292. https://doi.org/https://doi.org/10.1002/2015GB005332
Belkin, I.M., 2009. Rapid warming of large marine ecosystems. Prog. Oceanogr. 81, 207–213.
Bienfang, P.K., Szyper, J., Laws, E., 1983. Sinking rate and pigment responses to light-limitation of a marine diatom-implications to dynamics of chlorophyll maximum layers. Oceanol. acta 6, 55–62.
Burrows, M.T., Schoeman, D.S., Buckley, L.B., Moore, P., Poloczanska, E.S., Brander, K.M., Brown, C., Bruno, J.F., Duarte, C.M., Halpern, B.S., 2011. The pace of shifting climate in marine and terrestrial ecosystems. Science. 334, 652–655.
Butman, B., Aretxabaleta, A.L., Dickhudt, P.J., Dalyander, P.S., Sherwood, C.R., Anderson, D.M., Keafer, B.A., Signell, R.P., 2014. Investigating the importance of sediment resuspension in Alexandrium fundyense cyst population dynamics in the Gulf of Maine. Deep Sea Res. Part II Top. Stud. Oceanogr. 103, 79–95.
Chen, C., Huang, H., Beardsley, R.C., Xu, Q., Limeburner, R., Cowles, G.W., Sun, Y., Qi, J., Lin, H., 2011. Tidal dynamics in the Gulf of Maine and New England Shelf: An application of FVCOM. J. Geophys. Res. Ocean. 116, C12010. https://doi.org/10.1029/2011JC007054
Chen, C., Liu, H., Beardsley, R.C., 2003. An unstructured grid, finite-volume, three-dimensional, primitive equations ocean model: application to coastal ocean and estuaries. J. Atmos. Ocean. Technol. 20, 159–186.
Chen, C., Malanotte-Rizzoli, P., Wei, J., Beardsley, R.C., Lai, Z., Xue, P., Lyu, S., Xu, Q., Qi, J., Cowles, G.W., 2009. Application and comparison of kalman filters for coastal ocean problems: An experiment with FVCOM. J. Geophys. Res. Ocean. 114, C05011. https://doi.org/10.1029/2007JC004548
Chen, K., Gawarkiewicz, G.G., Lentz, S.J., Bane, J.M., 2014. Diagnosing the warming of the Northeastern U.S. Coastal Ocean in 2012: A linkage between the atmospheric jet stream variability and ocean response. J. Geophys. Res. Ocean. 119, 218–227. https://doi.org/10.1002/2013JC009393
Cranford, P.J., Gordon, D.C., 1992. The influence of dilute clay suspensions on sea scallop (Placopecten magellanicus) feeding activity and tissue growth. Netherlands J. Sea Res. 30, 107–120. https://doi.org/10.1016/0077-7579(92)90050-O
Damashek, J., Francis, C.A., 2018. Microbial Nitrogen Cycling in Estuaries: From Genes to Ecosystem Processes. Estuaries and Coasts 41, 626–660. https://doi.org/10.1007/s12237-017-0306-2
Dunne, J.P., Armstrong, R.A., Gnanadesikan, A., Sarmiento, J.L., 2005. Empirical and mechanistic models for the particle export ratio. Global Biogeochem. Cycles 19.
Eppley, R.W., 1972. Temperature and phytoplankton growth in the sea. Fish. Bull. 70, 1063–1085.
Fennel, K., Wilkin, J., Levin, J., Moisan, J., O'Reilly, J., Haidvogel, D., 2006. Nitrogen cycling in the Middle Atlantic Bight: Results from a three-dimensional model and implications for the North Atlantic nitrogen budget. Global Biogeochem. Cycles 20, GB3007. https://doi.org/10.1029/2005GB002456
Fennel, K., Wilkin, J., Previdi, M., Najjar, R., 2008. Denitrification effects on air-sea CO2 flux in the coastal ocean: Simulations for the northwest North Atlantic. Geophys. Res. Lett. 35, L24608. https://doi.org/10.1029/2008GL036147
Friedrichs, M.A.M., St-Laurent, P., Xiao, Y., Hofmann, E., Hyde, K., Mannino, A., Najjar, R.G.,

Narváez, D.A., Signorini, S.R., Tian, H., Wilkin, J., Yao, Y., Xue, J., 2019. Ocean Circulation Causes Strong Variability in the Mid-Atlantic Bight Nitrogen Budget. J. Geophys. Res. Ocean. 124, 113–134. https://doi.org/10.1029/2018JC014424

Geider, R.J., MacIntyre, H.L., Kana, T.M., 1997. Dynamic model of phytoplankton growth and acclimation: Responses of the balanced growth rate and the chlorophyll a:carbon ratio to light, nutrient-limitation and temperature. Mar. Ecol. Prog. Ser. 148, 187–200. https://doi.org/10.3354/meps148187

Gemmell, B.J., Oh, G., Buskey, E.J., Villareal, T.A., 2016. Dynamic sinking behaviour in marine phytoplankton: Rapid changes in buoyancy may aid in nutrient uptake. Proc. R. Soc. B Biol. Sci. 283, 20161126. https://doi.org/10.1098/rspb.2016.1126

Gentleman, W., Leising, A., Frost, B., Strom, S., Murray, J., 2003. Functional responses for zooplankton feeding on multiple resources: A review of assumptions and biological dynamics. Deep. Res. Part II 50, 2847–2875. https://doi.org/10.1016/j.dsr2.2003.07.001

Goode, A.G., Brady, D.C., Steneck, R.S., Wahle, R.A., 2019. The brighter side of climate change: How local oceanography amplified a lobster boom in the Gulf of Maine. Glob. Chang. Biol. 25, 3906–3917. https://doi.org/10.1111/gcb.14778

Griffiths, J.R., Kadin, M., Nascimento, F.J.A., Tamelander, T., Törnroos, A., Bonaglia, S., Bonsdorff, E., Brüchert, V., Gårdmark, A., Järnström, M., Kotta, J., Lindegren, M., Nordström, M.C., Norkko, A., Olsson, J., Weigel, B., Žydelis, R., Blenckner, T., Niiranen, S., Winder, M., 2017. The importance of benthic–pelagic coupling for marine ecosystem functioning in a changing world. Glob. Chang. Biol. 23, 2179–2196. https://doi.org/10.1111/gcb.13642

Hu, S., Chen, C., Ji, R., Townsend, D.W., Tian, R., Beardsley, R.C., Davis, C.S., 2011. Effects of surface forcing on interannual variability of the fall phytoplankton bloom in the gulf of maine revealed using a process-oriented model. Mar. Ecol. Prog. Ser. 427, 29–49. https://doi.org/10.3354/meps09043

Hu, S., Townsend, D.W., Chen, C., Cowles, G., Beardsley, R.C., Ji, R., Houghton, R.W., 2008. Tidal pumping and nutrient fluxes on Georges Bank: A process-oriented modeling study. J. Mar. Syst. 74, 528–544. https://doi.org/10.1016/j.jmarsys.2008.04.007

Hyde, K.J.W., O'Reilly, J.E., Oviatt, C.A., 2007. Validation of SeaWiFS chlorophyll a in Massachusetts Bay. Cont. Shelf Res. 27, 1677–1691. https://doi.org/10.1016/j.csr.2007.02.002

Ji, R., Davis, C., Chen, C., Beardsley, R., 2008a. Influence of local and external processes on the annual nitrogen cycle and primary productivity on Georges Bank: A 3-D biological-physical modeling study. J. Mar. Syst. 73, 31–47. https://doi.org/10.1016/j.jmarsys.2007.08.002

Ji, R., Davis, C.S., Chen, C., Townsend, D.W., Mountain, D.G., Beardsley, R.C., 2008b. Modeling the influence of low-salinity water inflow on winter-spring phytoplankton dynamics in the Nova Scotian Shelf–Gulf of Maine region. J. Plankton Res. 30, 1399–1416.

Ji, R., Davis, C.S., Chen, C., Townsend, D.W., Mountain, D.G., Beardsley, R.C., 2007. Influence of ocean freshening on shelf phytoplankton dynamics. Geophys. Res. Lett. 34, L24607. https://doi.org/10.1029/2007GL032010

Laurent, A., Fennel, K., Wilson, R., Lehrter, J., Devereux, R., 2016. Parameterization of biogeochemical sediment-water fluxes using in situ measurements and a diagenetic model. Biogeosciences 13, 77–94. https://doi.org/10.5194/bg-13-77-2016

Li, W.K.W., Glen Harrison, W., Head, E.J.H., 2006. Coherent assembly of phytoplankton

communities in diverse temperate ocean ecosystems. Proc. R. Soc. 273, 1953–1960.
Li, Y., Fratantoni, P.S., Chen, C., Hare, J.A., Sun, Y., Beardsley, R.C., Ji, R., 2015. Spatio-temporal patterns of stratification on the Northwest Atlantic shelf. Prog. Oceanogr. 134, 123–137. https://doi.org/10.1016/j.pocean.2015.01.003
Loder, J.W., 1998. The coastal ocean off northeastern North America: A large-scale view. In: Robinson, A.R.,Brink, K.H. (Eds.), . In: The Sea, vol. 11. John Wiley, New York, pp. 105-133.
Loder, J.W., Van Der Baaren, A., Yashayaev, I., 2015. Climate Comparisons and Change Projections for the Northwest Atlantic from Six CMIP5 Models. Atmosphere-Ocean. 53, 529–555. https://doi.org/10.1080/07055900.2015.1087836
Malone, T.C., Hopkins, T.S., Falkowski, P.G., Whitledge, T.E., 1983. Production and transport of phytoplankton biomass over the continental shelf of the new york bight. Cont. Shelf Res. 1, 305–337. https://doi.org/10.1016/0278-4343(83)90001-8
Margalef, R., 1978. Life-forms of phytoplankton as survival alternatives in an unstable environment. Oceanol. acta 1, 493–509.
Maritorena, S., d'Andon, O.H.F., Mangin, A., Siegel, D.A., 2010. Merged satellite ocean color data products using a bio-optical model: Characteristics, benefits and issues. Remote Sens. Environ. 114, 1791–1804. https://doi.org/10.1016/j.rse.2010.04.002
Miles, T., Seroka, G., Kohut, J., Schofield, O., Glenn, S., 2015. Glider observations and modeling of sediment transport in Hurricane Sandy. J. Geophys. Res. Ocean. 120, 1771–1791. https://doi.org/10.1002/2014JC010474
Mills, K.E., Pershing, A.J., Brown, C.J., Chen, Y., Chiang, F.S., Holland, D.S., Lehuta, S., Nye, J.A., Sun, J.C., Thomas, A.C., Wahle, R.A., 2013. Fisheries management in a changing climate: Lessons from the 2012 ocean heat wave in the Northwest Atlantic. Oceanography. 26, 191–195. https://doi.org/10.5670/oceanog.2013.27
Moriarty, J.M., Harris, C.K., Friedrichs, M.A.M., Fennel, K., Xu, K., 2018. Impact of seabed resuspension on oxygen and nitrogen dynamics in the northern Gulf of Mexico: A numerical modeling study. J. Geophys. Res. Ocean. 123, 7237– 7263. https://doi.org/10.1029/2018JC013950
Mountain, D.G., Manning, J.P., 1994. Seasonal and interannual variability in the properties of the surface waters of the Gulf of Maine. Cont. Shelf Res. 14, 1555–1581. https://doi.org/10.1016/0278-4343(94)90090-6
Mouw, C.B., Yoder, J.A., 2010. Optical determination of phytoplankton size composition from global SeaWiFS imagery. J. Geophys. Res. Ocean. 115, C12018. https://doi.org/10.1029/2010JC006337
Mouw, C.B., Yoder, J.A., 2005. Primary production calculations in the Mid-Atlantic Bight, including effects of phytoplankton community size structure. Limnol. Oceanogr. 50, 1232–1243. https://doi.org/10.4319/lo.2005.50.4.1232
O'Reilly, J.E., Busch, D.A., 1984. Phytoplankton primary production on the northwestern Atlantic shelf. Rapp. PV Reun. Cons. Int. Explor. Mer 183, 255–268.
O'Reilly, J.E., Zetlin, C.A., 1998. Seasonal, horizontal, and vertical distribution of phytoplankton chlorophyll a in the northeast US continental shelf ecosystem, NOAA Technical Report NMFS 139, U.S. Dep. of Commer., Seattle.
Pan, X., Mannino, A., Marshall, H.G., Filippino, K.C., Mulholland, M.R., 2011. Remote sensing of phytoplankton community composition along the northeast coast of the United States. Remote Sens. Environ. 115, 3731–3747. https://doi.org/10.1016/j.rse.2011.09.011

Pershing, A.J., Alexander, M.A., Hernandez, C.M., Kerr, L.A., Le Bris, A., Mills, K.E., Nye, J.A., Record, N.R., Scannell, H.A., Scott, J.D., Sherwood, G.D., Thomas, A.C., 2015. Slow adaptation in the face of rapid warming leads to collapse of the Gulf of Maine cod fishery. Science. 350, 809–812.

Pershing, A.J., Stamieszkin, K., 2020. The North Atlantic Ecosystem, from Plankton to Whales. Ann. Rev. Mar. Sci. 12, 339–359. https://doi.org/10.1146/annurev-marine-010419-010752

Ramp, S.R., Schlitz, R.J., Wright, W.R., 1985. The deep flow through the Northeast Channel, Gulf of Maine. J. Phys. Oceanogr. 15, 1790–1808.

Rebuck, N.D., Townsend, D.W., 2014. A climatology and time series for dissolved nitrate in the Gulf of Maine region. Deep. Res. Part II Top. Stud. Oceanogr. 103, 223–237. https://doi.org/10.1016/j.dsr2.2013.09.006

Ross, O.N., 2006. Particles in motion: How turbulence affects plankton sedimentation from an oceanic mixed layer. Geophys. Res. Lett. 33, L10609. https://doi.org/10.1029/2006GL026352

Ryan, J.P., Yoder, J.A., Cornillon, P.C., 1999. Enhanced chlorophyll at the shelfbreak of the Mid-Atlantic Bight and Georges Bank during the spring transition. Limnol. Oceanogr. 44, 1–11.

Schoudel, A., 1996. The seasonal variation of nutrients in three Maine estuaries. M.Sc. Thesis, University of New Hampshire, Durham, NH. 103.

Shearman, R.K., Lentz, S.J., 2010. Long-term sea surface temperature variability along the US East Coast. J. Phys. Oceanogr. 40, 1004–1017.

Sherman, E., Moore, J.K., Primeau, F., Tanouye, D., 2016. Temperature influence on phytoplankton community growth rates. Global Biogeochem. Cycles 30, 550–559. https://doi.org/10.1002/2015GB005272.Received

Song, H., Ji, R., Stock, C., Kearney, K., Wang, Z., 2011. Interannual variability in phytoplankton blooms and plankton productivity over the Nova Scotian Shelf and in the Gulf of Maine. Mar. Ecol. Prog. Ser. 426, 105–118. https://doi.org/10.3354/meps09002

Song, H., Ji, R., Stock, C., Wang, Z., 2010. Phenology of phytoplankton blooms in the Nova Scotian Shelf-Gulf of Maine region: Remote sensing and modeling analysis. J. Plankton Res. 32, 1485–1499. https://doi.org/10.1093/plankt/fbq086

Staehr, P.A., Birkeland, M.J., 2006. Temperature acclimation of growth, photosynthesis and respiration in two mesophilic phytoplankton species. Phycologia 45, 648–656. https://doi.org/10.2216/06-04.1

Staudinger, M.D., Mills, K.E., Stamieszkin, K., Record, N.R., Hudak, C.A., Allyn, A., Diamond, A., Friedland, K.D., Golet, W., Henderson, M.E., Hernandez, C.M., Huntington, T.G., Ji, R., Johnson, C.L., Johnson, D.S., Jordaan, A., Kocik, J., Li, Y., Liebman, M., Nichols, O.C., Pendleton, D., Richards, R.A., Robben, T., Thomas, A.C., Walsh, H.J., Yakola, K., 2019. It's about time: A synthesis of changing phenology in the Gulf of Maine ecosystem. Fish. Oceanogr. 28, 532–566. https://doi.org/10.1111/fog.12429

Stock, C.A., Dunne, J., 2010. Controls on the ratio of mesozooplankton production to primary production in marine ecosystems. Deep. Res. Part I Oceanogr. Res. Pap. 57, 95–112. https://doi.org/10.1016/j.dsr.2009.10.006

Stock, C.A., Powell, T.M., Levin, S.A., 2008. Bottom-up and top-down forcing in a simple size-structured plankton dynamics model. J. Mar. Syst. 74, 134–152. https://doi.org/10.1016/j.jmarsys.2007.12.004

Sun, Y., Chen, C., Beardsley, R.C., Ullman, D., Butman, B., Lin, H., 2016. Surface circulation in

Block Island Sound and adjacent coastal and shelf regions: A FVCOM-CODAR comparison. Prog. Oceanogr. 143, 26–45.
Sun, Y., Chen, C., Beardsley, R.C., Xu, Q., Qi, J., Lin, H., 2013. Impact of current-wave interaction on storm surge simulation: A case study for Hurricane Bob. J. Geophys. Res. Ocean. 118, 2685–2701. https://doi.org/10.1002/jgrc.20207
Switzer, M., Townsend, D., Pettigrew, N., 2020. The effects of source water masses and internal recycling on concentrations of dissolved inorganic nutrients in the Gulf of Maine. Cont. Shelf Res. 104157. https://doi.org/10.1016/j.csr.2020.104157
Thomas, A.C., Pershing, A.J., Friedland, K.D., Nye, J.A., Mills, K.E., Alexander, M.A., Record, N.R., Weatherbee, R., Elisabeth Henderson, M., 2017. Seasonal trends and phenology shifts in sea surface temperature on the North American northeastern continental shelf. Elem. Sci. Anthr. 5, 48. https://doi.org/10.1525/elementa.240
Thomas, A.C., Townsend, D.W., Weatherbee, R., 2003. Satellite-measured phytoplankton variability in the Gulf of Maine. Cont. Shelf Res. 23, 971–989. https://doi.org/10.1016/S0278-4343(03)00086-4
Thomas, M.K., Kremer, C.T., Klausmeier, C.A., Litchman, E., 2012. A global pattern of thermal adaptation in marine phytoplankton. Science. 338, 1085–1088. https://doi.org/10.1126/science.1224836
Tian, R., Chen, C., Qi, J., Ji, R., Beardsley, R.C., Davis, C., 2014. Model study of nutrient and phytoplankton dynamics in the Gulf of Maine: Patterns and drivers for seasonal and interannual variability. ICES J. Mar. Sci. 72, 388–402. https://doi.org/10.1093/icesjms/fsu090
Townsend, D.W., 1998. Sources and cycling of nitrogen in the Gulf of Maine. J. Mar. Syst. 16, 283–295. https://doi.org/10.1016/S0924-7963(97)00024-9
Townsend, D.W., Cammen, L.M., 1988. Potential importance of the timing of spring plankton blooms to benthic-pelagic coupling and recruitment of juvenile demersal fishes. Biol. Oceanogr. 5, 215–228.
Townsend, D.W., McGillicuddy, D.J., Thomas, M.A., Rebuck, N.D., 2014. Nutrients and water masses in the Gulf of Maine-Georges Bank region: Variability and importance to blooms of the toxic dinoflagellate Alexandrium fundyense. Deep. Res. Part II Top. Stud. Oceanogr. 103, 238–263. https://doi.org/10.1016/j.dsr2.2013.08.003
Townsend, D.W., Rebuck, N.D., Thomas, M.A., Karp-Boss, L., Gettings, R.M., 2010. A changing nutrient regime in the Gulf of Maine. Cont. Shelf Res. 30, 820–832. https://doi.org/10.1016/j.csr.2010.01.019
Townsend, D.W., Thomas, A.C., Mayer, L.M., Thomas, M.A., Quinlan, J.A., 2006. Oceanography of the northwest Atlantic continental shelf. In: Robinson, A.R., Brink, K.H. (Eds.), The Sea, vol. 14. Harvard University Press. (pp. 119-168).
Van Oostende, N., Dussin, R., Stock, C.A., Barton, A.D., Curchitser, E., Dunne, J.P., Ward, B.B., 2018. Simulating the ocean's chlorophyll dynamic range from coastal upwelling to oligotrophy. Prog. Oceanogr. 168, 232–247. https://doi.org/10.1016/j.pocean.2018.10.009
Xu, Y., Chant, R., Gong, D., Castelao, R., Glenn, S., Schofield, O., 2011. Seasonal variability of chlorophyll a in the Mid-Atlantic Bight. Cont. Shelf Res. 31, 1640–1650. https://doi.org/10.1016/j.csr.2011.05.019
Yoder, J.A., O'Reilly, J.E., Barnard, A.H., Moore, T.S., Ruhsam, C.M., 2001. Variability in coastal zone color scanner (CZCS) Chlorophyll imagery of ocean margin waters off the US East Coast. Cont. Shelf Res. 21, 1191–1218.

Yoder, J.A., Schollaert, S.E., O'Reilly, J.E., 2002. Climatological phytoplankton chlorophyll and sea surface temperature patterns in continental shelf and slope waters off the northeast U.S. coast. Limnol. Oceanogr. 47, 672–682. https://doi.org/10.4319/lo.2002.47.3.0672

Zhang, S., Stock, C.A., Curchitser, E.N., Dussin, R., 2019. A Numerical Model Analysis of the Mean and Seasonal Nitrogen Budget on the Northeast U.S. Shelf. J. Geophys. Res. Ocean. 124, 2969–2991. https://doi.org/10.1029/2018JC014308

Zhang, W.G., McGillicuddy, D.J., Gawarkiewicz, G.G., 2013. Is biological productivity enhanced at the New England shelfbreak front? J. Geophys. Res. Ocean. 118, 517–535. https://doi.org/10.1002/jgrc.20068

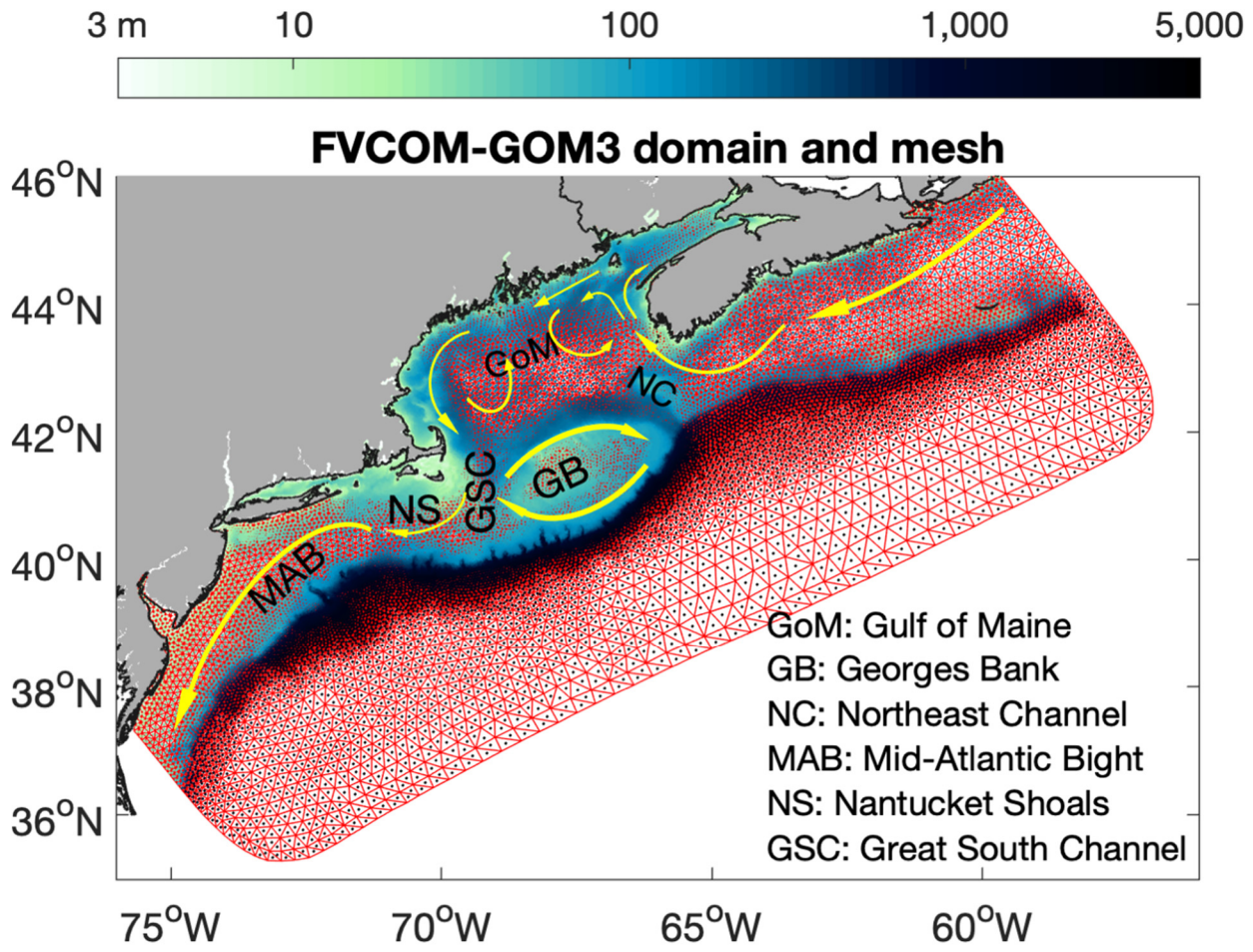

Fig. 1. FVCOM model domain and unstructured triangular mesh (red lines) for the Northwest Atlantic Shelf. The color of cell centers (dots) represents water depth. Yellow arrows represent surface circulation patterns over the shelf.

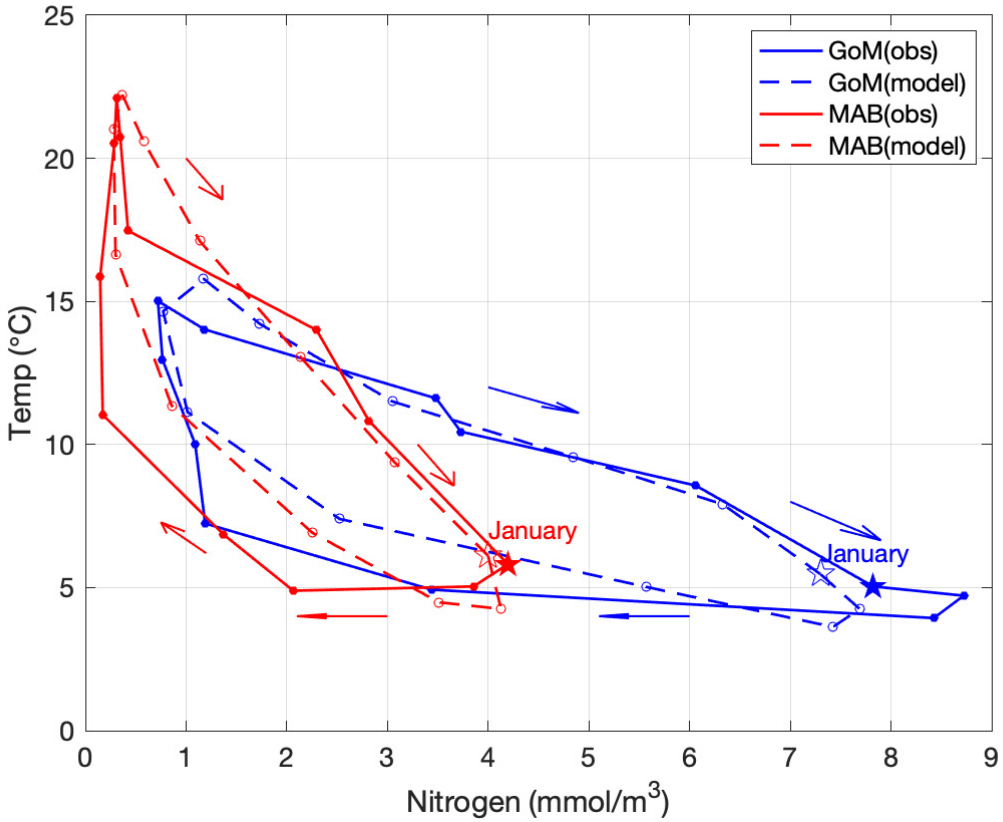

Fig. 2. Annual cycle of temperature versus nitrogen concentration over the top 10 m in the GoM (blue) and the MAB (red). The solid lines are based on monthly observations and the dashed lines are based on model results. The stars represent January and circles represent other months. The direction of annual cycle is clockwise.

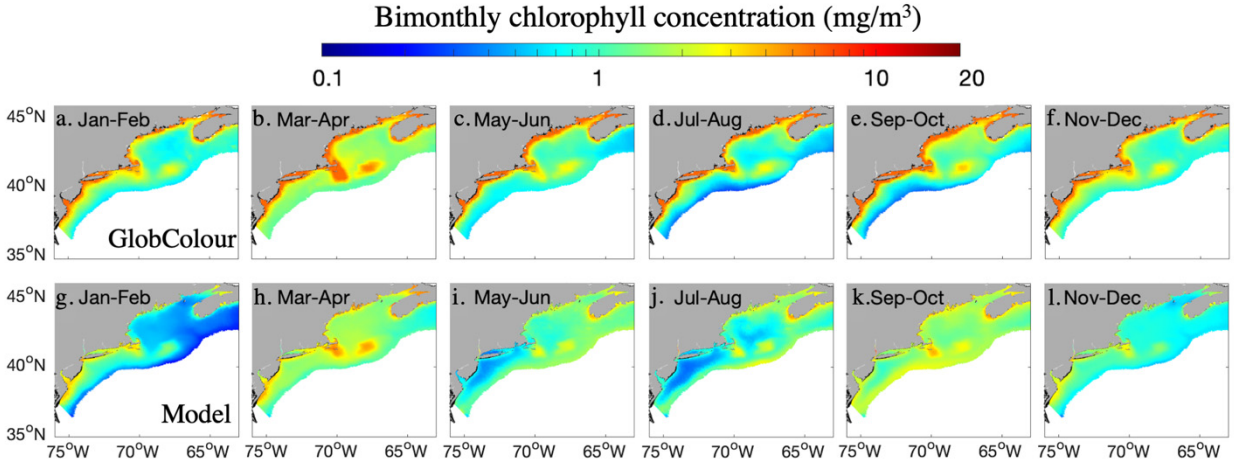

Fig. 3. Bimonthly chlorophyll concentration comparison between GlobColour (upper panels) and model results over the top 10 m (lower panels). The cutoff water depth is 1000 m.

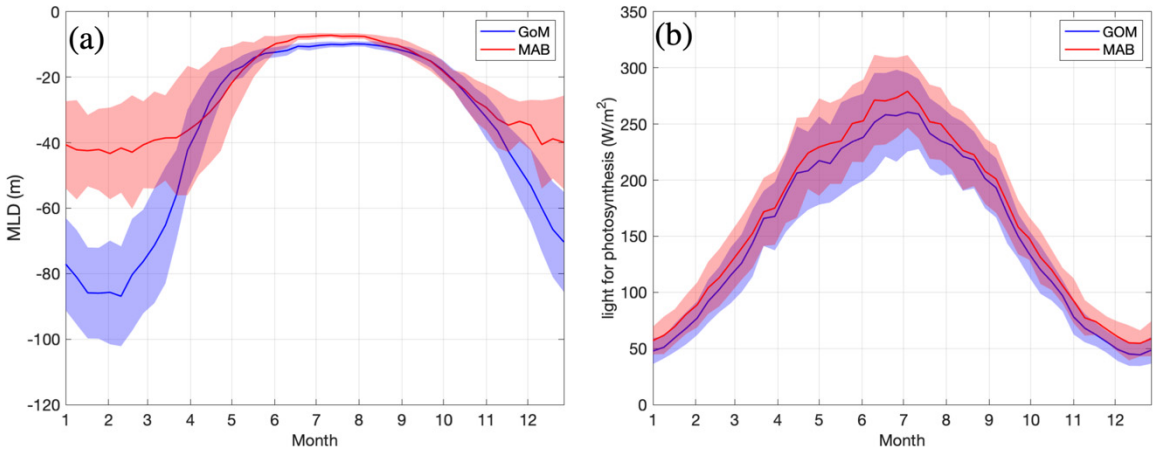

Fig. 4. spatial mean of mixed layer depth (a) and light for photosynthesis (b) climatology (8-day composite) in the GoM and the MAB. Shaded areas represent one standard deviation.

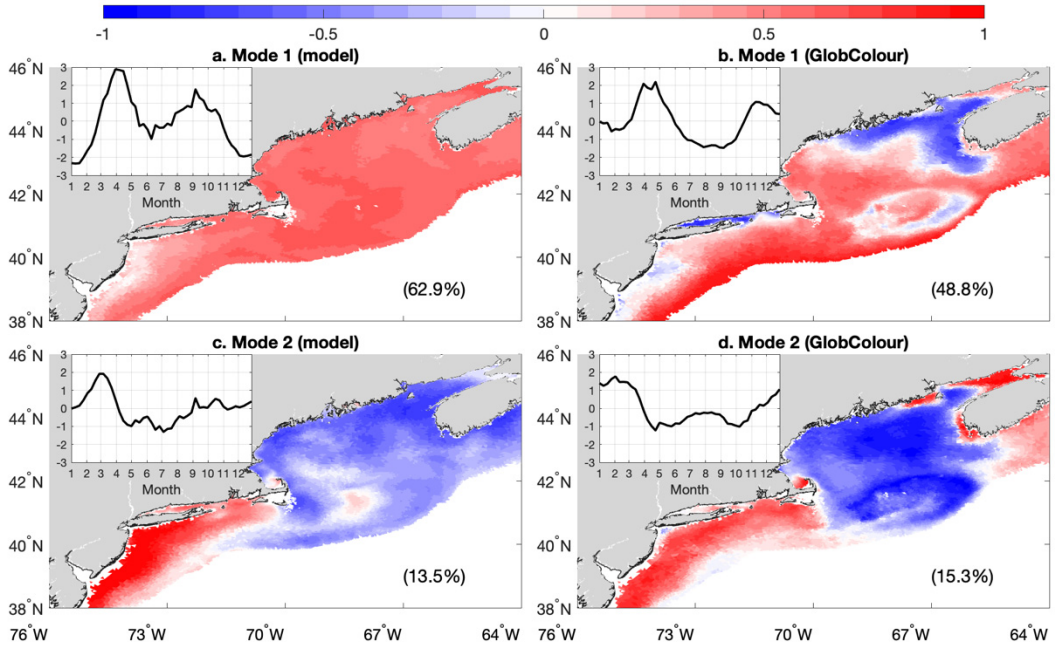

Fig. 5. Spatial patterns of EOF analysis based on the normalized modeled (left column) and GlobColour (right column) surface chlorophyll concentration with the corresponding time series (upper left of each panel) and the percentage of variability explained by each mode (lower right corner of each panel). The upper two panels represent the first mode and the lower two panels represent the second mode, respectively.

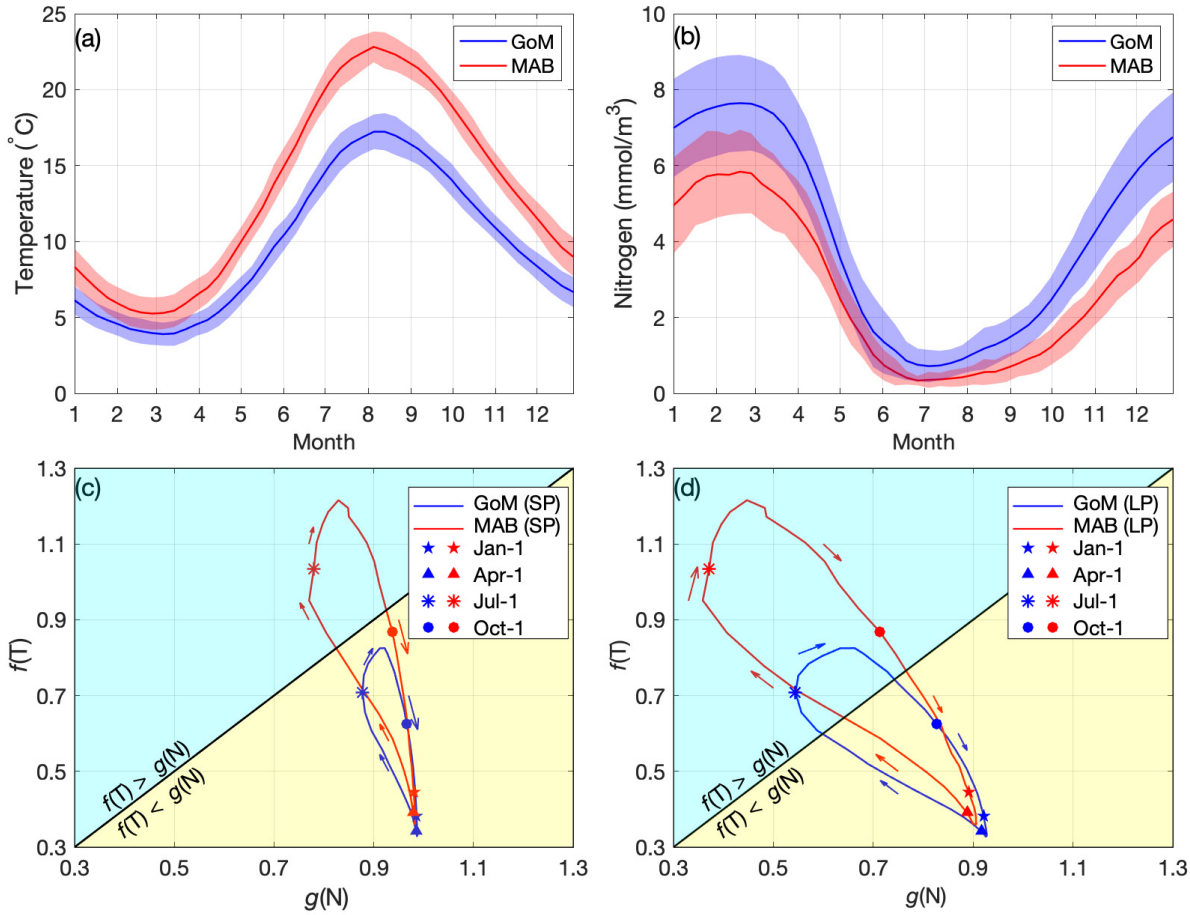

Fig. 6. The upper two panels show spatial mean of water temperature (a) and nutrient (b) climatology (8-day composite) over the top 10 m in the GoM and the MAB. Shaded areas depict one standard deviation. The lower two panels represent annual cycle of nutrient limit term $g(N)$ versus temperature limit term $f(T)$ for small phytoplankton (SP; panel c) and large phytoplankton (LP; panel d). In cyan area, nutrient limitation outweighs temperature limitation ($f(T) > g(N)$). In yellow area, nutrient limitation is weaker than temperature limitation ($f(T) < g(N)$). The direction of annual cycle is clockwise.

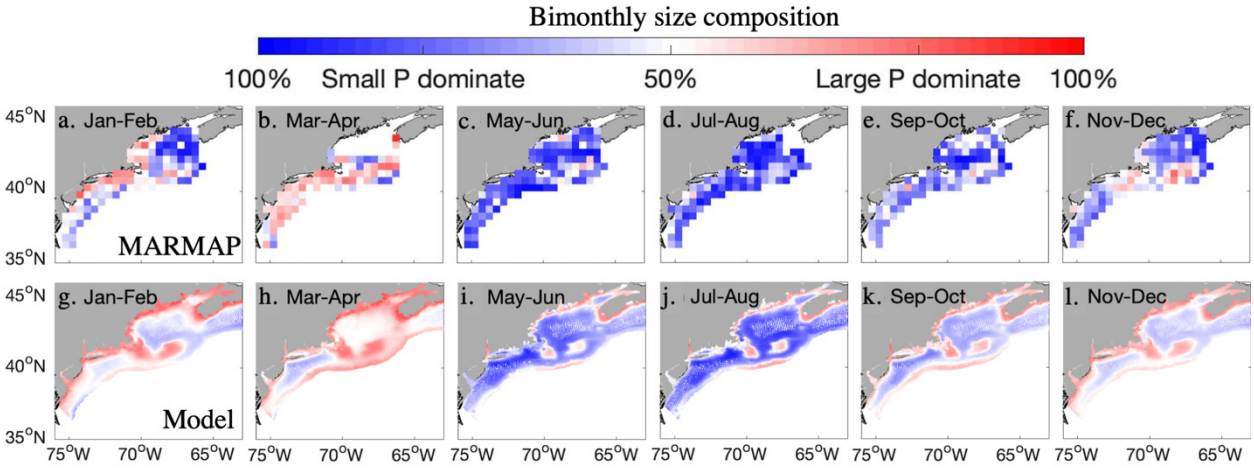

Fig. 7. Bimonthly phytoplankton size structure comparison between MARMAP dataset (upper panels) and model results over the top 10 m (lower panels). The cutoff water depth is 1000 m.

.

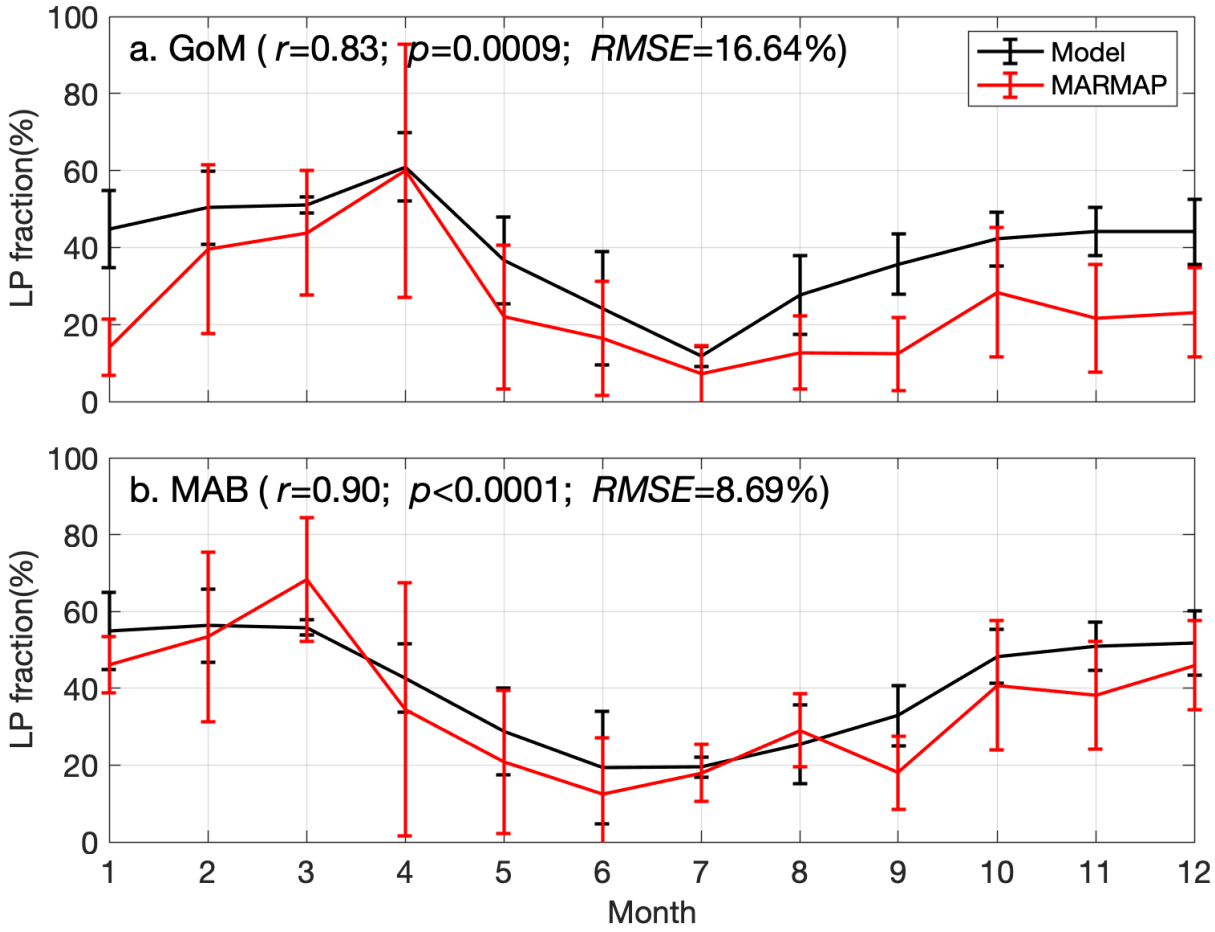

Fig. 8. Modeled (black) and MARMAP (red) monthly time series of large phytoplankton (LP) fraction in the GoM (a) and MAB (b). Error bars indicate one standard deviation.

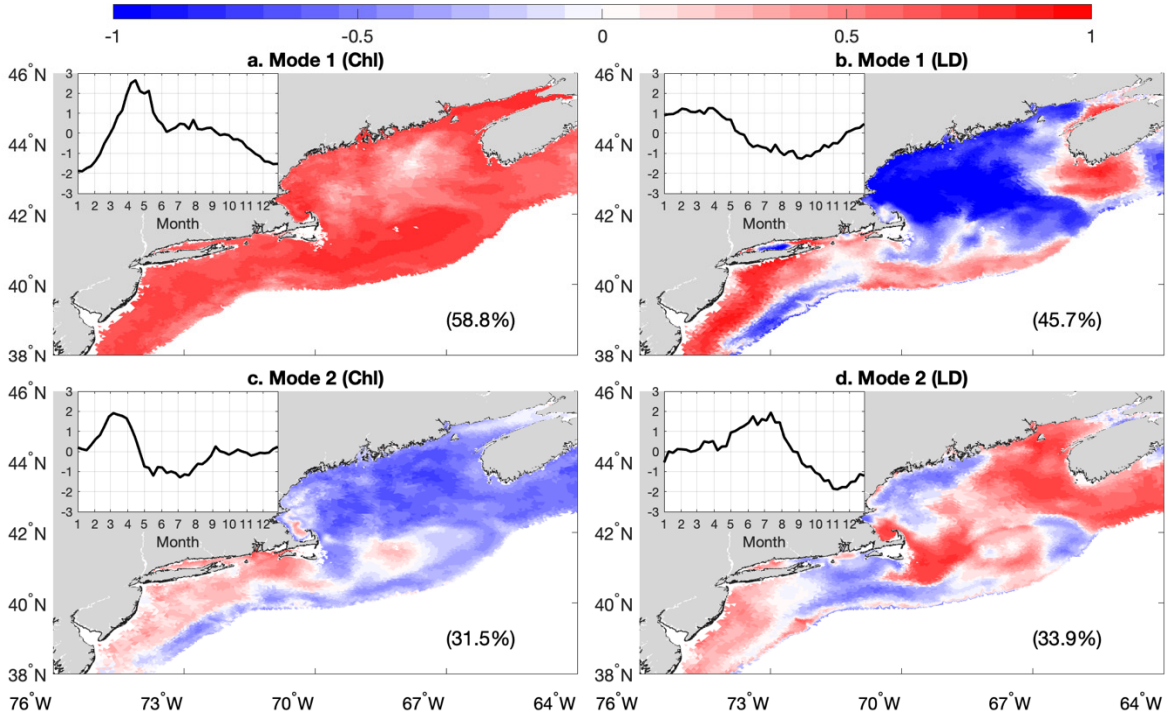

Fig. 9. Spatial patterns of EOF analysis based on the modeled chlorophyll concentration (left column) and large detritus concentration (right column) at the bottom with the corresponding time series (upper left of each panel) and the percentage of variability explained by each mode (lower right corner of each panel). The upper two panels represent the first mode and the lower two panels represent the second mode, respectively.

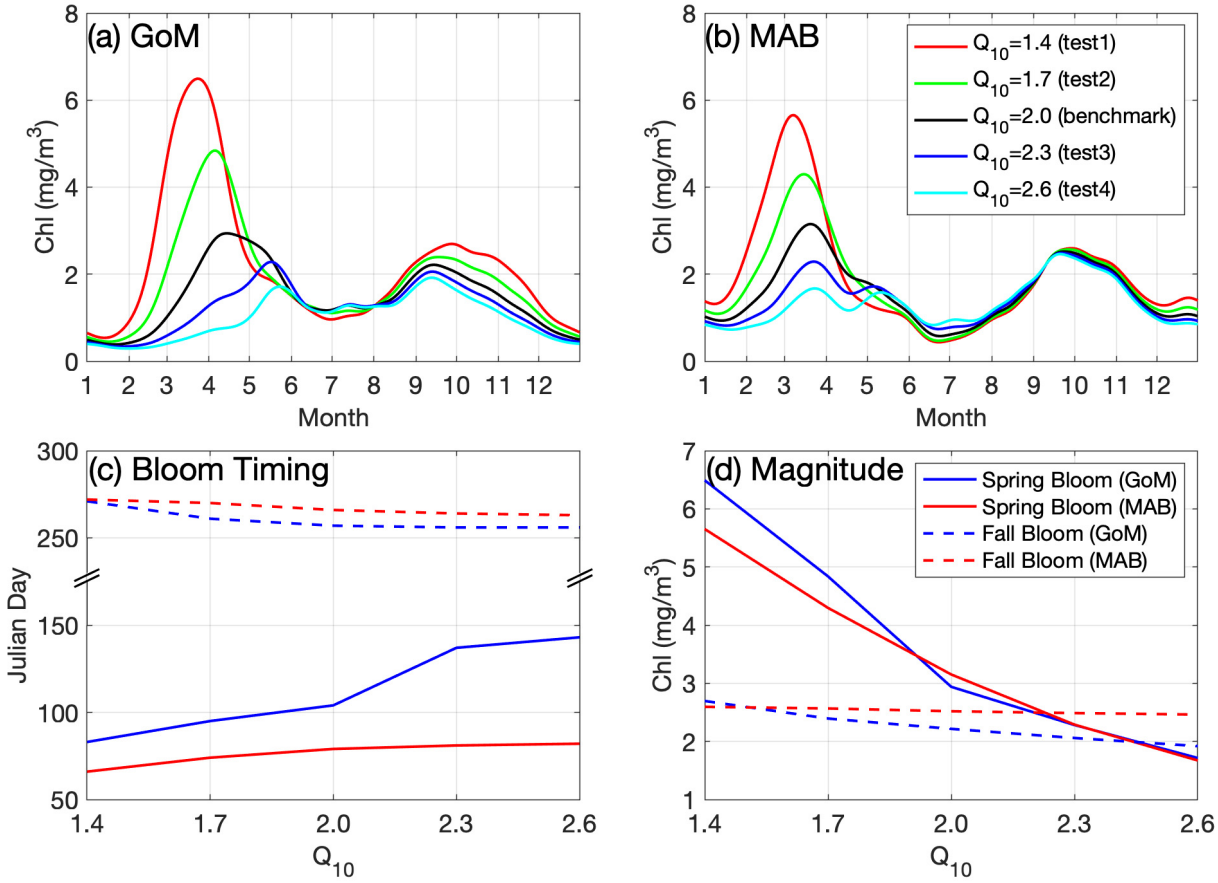

Fig. 10. Comparison of spatial averaged chlorophyll concentration over the top 10 m between the benchmark run (black line) and sensitivity tests with different Q_{10} in the GoM (a) and the MAB (b). A Gaussian smoothing was applied to model results following Ji et al. (2007) for detecting bloom timing (c) and magnitude (d).